The effect of the range of the potential on the structures of clusters

Jonathan P. K. Doye, David J. Wales, and R. Stephen Berry

Citation: The Journal of Chemical Physics **103**, 4234 (1995); doi: 10.1063/1.470729
View online: http://dx.doi.org/10.1063/1.470729
View Table of Contents: http://scitation.aip.org/content/aip/journal/jcp/103/10?ver=pdfcov
Published by the AIP Publishing

The effect of the range of the potential on the structures of clusters

Jonathan P. K. Doye and David J. Wales
University Chemical Laboratories, Lensfield Road, Cambridge CB2 1EW, United Kingdom

R. Stephen Berry
Department of Chemistry, University of Chicago, 5735 South Ellis Avenue, Chicago, Illinois 60637

(Received 12 April 1995; accepted 2 June 1995)

We investigate the structures of clusters bound by the Morse potential by mapping the structure of the global minimum as a function of both cluster size and the range of the pair potential. We consider values of the range parameter appropriate to a loosely bound diatomic molecule (longest), two C_{60} molecules (shortest), and at regular intervals between these two limits. We have studied all cluster sizes with 25 atoms or less and a selection of sizes containing between 35 and 80 atoms. The effect of decreasing the range of the potential is to destabilize strained structures. For the larger clusters the structure of the global minimum changes from icosahedral to decahedral to face-centered cubic as the range is decreased. We have also investigated the effects of temperature on the equilibrium structure by performing a model calculation for a 75-atom cluster. © *1995 American Institute of Physics.*

I. INTRODUCTION

A longstanding but perhaps imprecisely posed question in cluster science is ''What is the structure of a particular cluster?.'' Sometimes we mean ''What is the structure of this cluster at the global minimum of its potential energy surface?'' or, equivalently, ''What is the structure of this cluster at zero Kelvin?'' At other times, the question is better phrased as ''What is the general category of structure that this kind of cluster will have at a specified temperature?'' Questions of this kind arose as soon as it became clear that rare gas clusters tend to exhibit structures based upon icosahedral geometries, while the corresponding bulk solids have close-packed, face-centered cubic (fcc) structures. Naturally this stimulated investigations of the size dependence of structures; many people sought to find where and how, as a function of cluster size, the transition occurs from icosahedral to cubic.[1–5] This study is, in part, a continuation of that issue, which is still not fully resolved.

Another dimension to the question of what controls structure is the nature of the interaction among the particles. How the form of the potential determines the lowest and the other low-lying potential energy minima is the main focus of this investigation. Many studies have concentrated on the structures of clusters exhibited by a specific functional form, such as the Lennard-Jones (LJ) potential.[6] Fewer have examined the general structural effects of the different contributions to the potential. For this purpose, it is useful to consider a potential which is simple enough that we can comprehend the effects of any changes we make to its form, and where these changes can be made by varying a single parameter. This method has been used to investigate the effect of the range[7–9] and anisotropy[10] of the potential on the structure and phase behavior of small clusters.

Braier *et al.*[7] made a systematic search of the potential energy surface (PES) of six- and seven-atom clusters bound by the Morse potential[11] as a function of the range of the interaction. They found that as the range was increased the number of minima and saddle points on the PES decreased and the PES became smoother and simpler. This effect was first noted by Hoare and McInnes in comparisons of LJ and long-ranged Morse clusters,[12,13] and has been further illustrated for binary salt clusters such as potassium chloride by the use of a shielded Coulomb potential for the long-range term of a Born–Mayer potential.[14] This simplification of the PES for long-range interactions led Stillinger and Stillinger[15] to suggest that increasing the range of a potential may provide a suitable method of hypersurface deformation to facilitate global optimization.[16]

Bytheway and Kepert noted that, for a sufficiently long-ranged potential, structures based on icosahedral packings become less favored energetically than structures with even higher coordination.[8] Little, however, has been discovered about the structures associated with shorter-ranged potentials, and the effects of the range and size on the competition among icosahedral, decahedral, and close-packed structures. Here we investigate these issues by examining clusters of particles bound by the Morse potential. We consider all clusters containing up to 25 atoms and a selection with sizes in the range 35–80. In particular, we attempt to find the global minimum as a function of the range and size.

A useful comparison is provided by the structures already known for specific systems. Metal clusters often have long-ranged interactions, LJ clusters medium-ranged and clusters of C_{60} molecules very short-ranged interactions, relative to the pair equilibrium separation. For example, in a study of nickel and palladium clusters, Stave and DePristo analyzed the structures they found in terms of the range of the potential.[17] In contrast, C_{60} has many interesting properties related to the short range of its intermolecular potential. It has been shown that the liquid phase of bulk C_{60} is unstable[18] or only marginally stable.[19] This discovery has led to a flurry of investigations of the effect of range on the phase diagram. These studies have shown that the liquid phase is destabilized as the range decreases[20–23] and that at very short ranges there may be a range-induced solid–solid transition similar to a liquid–vapor transition.[24,25] Clusters of C_{60} molecules have been shown to have structures very different from those of the corresponding LJ clusters.[26–28]

The structure of LJ clusters has been the subject of in-

 0021-9606/95/103(10)/4234/16/$6.00

tense study. Icosahedral clusters are the lowest in energy for small sizes. Northby has conducted a systematic survey for $13 \leqslant N \leqslant 147$ to find the lowest-energy minima based on icosahedral structures.[29] For larger systems sequences of magic number clusters with different structures have been compared. In these comparisons, the energy is interpolated between the values of N for the clusters of the sequence. The values of N at which the lowest-energy lines cross are indicators of the size for which a structural transition is likely to occur. These studies have shown that a decahedral sequence becomes most stable at $N \approx 1600$ and an fcc sequence[4] at $N \approx 10^5$. The energetics underlying this progression result from a balance between the lower surface energies and more spherical shape of the icosahedra and decahedra, and their inherent strain energies. The strain energies, as they are approximately proportional to the volume of the cluster, increase more rapidly with N than the surface energies. Therefore at some critical size the decahedral sequence becomes lower in energy than the icosahedral sequence because it is less strained. Similarly, because of the lack of strain in the fcc structures, the latter become lower in energy than the decahedra at a still larger size. Less is known about the stable structures in between the magic numbers. Our investigation will help to elucidate the basis for the favored structures in such systems.

II. METHODS

A. Potential

The Morse potential may be written as

$$V_{\mathrm{M}} = \epsilon \sum_{i<j} e^{\beta(r_0 - r_{ij})}(e^{\beta(r_0 - r_{ij})} - 2)$$

$$\equiv \sum_{i<j} e^{\rho_0(1 - r'_{ij})}(e^{\rho_0(1 - r'_{ij})} - 2),$$

where $\epsilon = 1$ and $r_0 = 1$ define the units of energy and length, respectively, $\rho_0 = \beta r_0$ and r'_{ij} denotes the distance between atoms i and j in these reduced units.[30] If the mass of the particles, m, is taken as the unit of mass then the reduced unit of time is $(mr_0^2/\epsilon)^{1/2}$. Here we denote an N-atom cluster bound by the Morse potential by M_N.

The parameter ρ_0 determines the range of the attractive part of the potential. As can be seen from Fig. 1 low values of ρ_0 give a long-ranged potential, and high values a short-ranged potential. ρ_0 also affects the steepness of the repulsive wall. The Morse and LJ potentials have the same curvature at the bottom of the well when $\rho_0 = 6$, and at this value the PES's have very similar topologies for six- and seven-atom clusters.[7] Girifalco has obtained an intermolecular potential for C_{60} molecules,[31] which is isotropic and short-ranged relative to the equilibrium pair separation, with an effective value[32] of $\rho_0 = 13.62$. The value of ρ_0 for nickel derived from bulk data[17] is 3.96. The alkali metals have even longer-ranged interactions. Appropriate values of ρ_0 are 3.17 for potassium and 3.15 for sodium.[33]

To understand the requirements for a structure to be low in energy and how these change with the value of the range parameter, ρ_0, it is instructive to look more closely at the form of the potential. The energy can be partitioned into three contributions as follows:

$$V_{\mathrm{M}} = -n_{nn} + E_{\mathrm{strain}} + E_{nnn}.$$

The number of nearest-neighbor contacts, n_{nn} is given by

$$n_{nn} = \sum_{i<j, x_{ij}<x_0} 1,$$

where $x_{ij} = r'_{ij} - 1$, and x_0 is a nearest-neighbor criterion. x_{ij} is the strain in the contact between atoms i and j. The strain energy, E_{strain}, is given by

$$E_{\mathrm{strain}} = \sum_{i<j, x_{ij}<x_0} (e^{-\rho_0 x_{ij}} - 1)^2.$$

The contribution to the energy from non-nearest-neighbors, E_{nnn}, is given by

$$E_{nnn} = \sum_{i<j, x_{ij}>x_0} e^{-\rho_0 x_{ij}}(e^{-\rho_0 x_{ij}} - 2).$$

The dominant term in the energy comes from n_{nn}. E_{nnn} is a smaller term and its value varies in a similar manner to n_{nn}. It is only likely to be important in determining the lowest-energy structures when other factors are equal. For example, bulk fcc and hexagonal close-packed (hcp) lattices both have 12 nearest-neighbors per atom. Next-nearest-neighbor interactions are the cause of the lower energy of the hcp crystal when a pair potential such as the LJ form is used.[34] Non-nearest-neighbor interactions also cause the contraction of nearest-neighbor distances from the equilibrium pair value. This contraction increases with the range of the potential.[35] At large values of ρ_0 (short range) the contribution from E_{nnn} is very small. The strain energy is likely to be an important factor in determining the favorable geometries as its value is very dependent on the structural type. Generally, more highly strained structures are able to have a higher value of n_{nn}. Hence, E_{strain} and n_{nn} are in competition. For a given strain, E_{strain} increases rapidly with ρ_0, as can be seen by taking a Taylor expansion of E_{strain} about $x_{ij} = 0$:

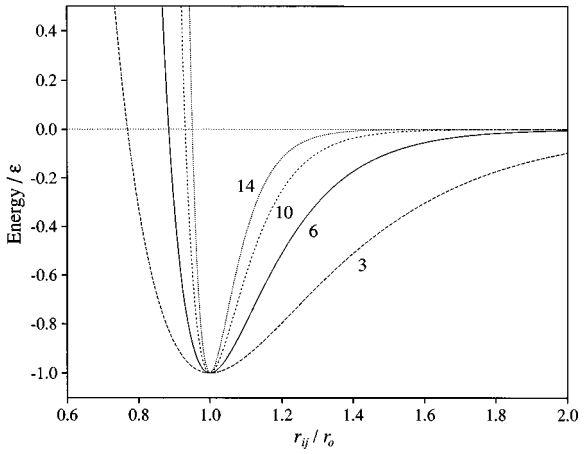

FIG. 1. Plots of the Morse potential for different values of ρ_0. Each line is labeled by its value of ρ_0.

$$E_{\text{strain}} \approx \sum_{i<j, x_{ij}<x_0} \rho_0^2 x_{ij}^2 - \rho_0^3 x_{ij}^3 + 7\rho_0^4 x_{ij}^4/12 + \cdots .$$

This expansion is valid when $\rho_0 x_{ij}$ is small. To a first approximation the strain energy grows quadratically with ρ_0. Thus, increasing ρ_0 destabilizes strained structures.

From this analysis we can see that minimization of the total energy involves a balance between maximization of n_{nn} and minimization of E_{strain}. This explains the observations of Bytheway and Kepert:[8] as the range of the potential increases (i.e., ρ_0 decreases) the potential becomes increasingly tolerant of strain, so there comes a point at which the energies of highly strained, but highly coordinated, structures become lower than icosahedral structures.

We can also predict the effect of the range on the competition between icosahedral, decahedral and fcc structures. The interior atoms of all three structures are twelve-coordinate. Differences in n_{nn} arise from differences in the coordination of surface atoms—{111} faces are more closely packed than {100} faces—and from differences in the fraction of atoms in the surface or equivalently in the sphericity of the cluster. The lowest-energy sequences for decahedral and fcc clusters[4] involve a balance between these two factors, whereas the icosahedron has entirely {111} faces and a nearly spherical shape. Consequently, of the above three morphologies, icosahedral structures have the largest n_{nn} and fcc usually have the smallest. However, icosahedral structures are also the most highly strained while fcc structures may be essentially unstrained if the pairwise forces are central. Hence, for a moderately long-ranged potential, icosahedral structures are the most stable. As ρ_0 is increased, the strain energy of the icosahedral structures increases rapidly, and there comes a point where the decahedral structure becomes more stable. Similarly, at still higher ρ_0 there comes a point where the fcc structure becomes most stable. The effect of decreasing the range of the potential is similar to the effect of increasing the number of atoms: both destabilize strained structures. The most favorable morphology can vary with the size of the cluster and the range of the potential.

The partitioning of the energy we have employed in this analysis is clear cut for the lattice based structures—there is an obvious gap in the pair distribution function between nearest and next-nearest-neighbor distances. However, for the structures favored when the potential is long ranged, this distinction becomes blurred and the cutoff used more arbitrary.

A similar partitioning has recently been employed by Smirnov (although he ignored E_{nnn}) in an analytical model, comparing the energies of icosahedral and fcc clusters.[36] Braier *et al.* have also noted that as $\rho_0 \to 0$, the energy simply becomes the total number of pairs of atoms in the cluster, $N(N-1)/2$, because all pairs then contribute the same energy, and that as $\rho_0 \to \infty$ the energy is the number of nearest-neighbor pairs at precisely the equilibrium pair distance.[7]

B. Searching the potential energy surface

We have used two methods to search for the global minimum of the PES. Using the physical insight gained from the analysis in the previous section we attempted to construct geometries that maximize n_{nn} based on a particular growth sequence. This method can be used for the lattice-based structures, but not for the highly strained structures at low ρ_0, where the concept of a lattice breaks down. This type of approach has been previously used by Harris *et al.*[37] to explain intensity peaks in the mass spectrum of charged argon clusters, and by Northby to generate possible global minimum structures for icosahedral LJ clusters.[29]

Second, we used molecular dynamics (MD) to explore the PES and to generate configurations for quenching.[38] The simulations employed the velocity Verlet algorithm[39] and configurations were quenched using an eigenvector-following[27] method. The trajectories usually consisted of 10^6 time steps, each of 0.004 24 reduced time units (10^{-14} s for parameters appropriate to Ar). When searching for new favorable geometries, the MD runs were performed at an energy corresponding to the upper end of the melting region. When searching for the lowest-energy minimum based on a particular morphology low-energy MD runs were initiated from that structure.

This MD technique is most effective when the surface is simple enough for it to be explored entirely on the time scale of the MD runs. As noted earlier, the effect of decreasing the range of the potential is to increase the number of minima and transition states on the surface, and also to increase the heights of the barriers between minima.[27] The number of minima on the PES also increases rapidly with the size of the system:[12,40] we estimate that for LJ_{55} the number of geometrically distinct minima[41] is of the order of 10^{21}. Hence, as N and ρ_0 increase, dynamic searching of the PES becomes increasingly difficult. However, this method was found to be effective for all but the larger clusters ($N \geqslant 70$).

The two methods we employed are complementary, the first generating starting points for MD runs and often reducing the problem to a local dynamic search of the PES, and the second generating new and unexpected structures not considered in the growth schemes. It must be emphasized, though, that these methods provide no guarantee that the global minimum has been found. Finding the global minimum for a PES with so many degrees of freedom is an NP-hard problem.[42] A global optimization approach, such as the method applied by Maranas and Floudas to small LJ clusters,[43] may provide a more rigorous assessment of the success of our project. However, their algorithm scales as 2^N, and has not yet been applied to the size regime of the larger clusters in this study. Recently, an optimization algorithm based on Glover's taboo search has been shown to hold promise.[44] Morse clusters would be an ideal system to compare different global optimization techniques because the complexity of the PES can be systematically varied by changing a single parameter, and this study provides some upper bounds for the global minima.

III. RESULTS

A. $M_2 - M_{25}$

For very small clusters the range of the potential has little effect on the global minimum. For $N=2$, 3, and 4 the energies of the optimal linear diatomic, equilateral triangle, and tetrahedron do not change with ρ_0. They are all maxi-

TABLE I. Global minima for $N \leqslant 25$. Energies at values of ρ_0 for which the structure is the global minimum are given in bold. $\rho_{\min}$ and $\rho_{\max}$ give the range of ρ_0 for which the structure is the global minimum. For 5A, 6A, and 7A no values are given, because they are global minima for all values of ρ_0 that we have considered. If, at a particular value of ρ_0 a structure is not a minimum, but a higher-order saddle point, the index of the stationary point (the number of negative eigenvalues of the Hessian) is given in square brackets after the energy. E_{strain} has been calculated at $\rho_0=10$. If a structure is not stable at $\rho_0=10$, no value of E_{strain} is given. All energies are given in ϵ.

	Point group	n_{nn}	E_{strain}	$\rho_0=3.0$	$\rho_0=6.0$	$\rho_0=10.0$	$\rho_0=14.0$	$\rho_{\min}$	$\rho_{\max}$
5A	D_{3h}	9	0.000	**−9.299 500**	**−9.044 930**	**−9.003 565**	**−9.000 283**		
6A	O_h	12	0.000	**−13.544 229**	**−12.487 810**	**−12.094 943**	**−12.018 170**		
7A	D_{5h}	16	0.062	**−17.552 961**	**−16.207 580**	**−15.956 512**	**−15.883 113**		
8A	D_{2d}	18	0.006	**−22.042 901**	−19.161 862	−18.275 118	−18.076 248		5.28
8B	C_s	19	0.062		**−19.327 420**	**−18.964 638**	**−18.883 688**	5.28	
9A	D_{3h}	21	0.002	**−26.778 449**	−22.330 837	−21.213 531	−21.037 957		5.50
9B	C_{2v}	22	0.062	−26.037 771	**−22.488 044**	**−21.975 747**	**−21.884 483**	5.50	
10A	D_{4d}	24	0.002	−31.519 768	−25.503 904	−24.204 958	−24.031 994		2.26
10B	C_{3v}	27	0.694	**−31.888 630**	**−27.473 283**	**−26.583 857**	**−26.132 735**	2.26	
11A	D_{4d}	34	10.374	**−37.930 817**	−28.795 153[4]	−23.666 072[5]			3.40
11B	C_{2v}	32		−37.891 674[1]				3.40	3.67
11C	C_{2v}	31	0.792		**−31.521 880**	**−30.265 230**	−29.588 130[1]	3.67	13.57
11D	C_s	30					**−29.596 054**	13.57	15.29
11E	C_2	30	0.248	−36.613 190[1]	−30.698 890	−29.808 994	−29.524 398	15.29	20.59
11F	C_{2v}	29	0.001	−36.697 760	−30.431 713	−29.215 51	−29.037 941	20.59	
12A	C_{2v}	38		−43.971 339[1]	−35.199 881[1]				2.67
12B	C_{5v}	36	1.704	**−44.097 880**	**−36.400 278**	**−34.366 755**	−33.115 942[1]	2.67	12.15
12C	C_s	34					−33.199 505	12.15	13.03
12D	D_{2d}	34	0.346	−41.816 393	−34.838 761	−33.724 155	**−33.332 305**	13.03	17.08
12E	D_{3h}	33	0.001	−42.121 440	−34.568 002	−33.222 331	−33.038 298	17.08	
13A	I_h	42	2.425	**−51.737 046**	**−42.439 863**	**−39.662 975**	**−37.258 877**		14.76
13B	D_{5h}	37	0.141	−49.998 058[1]	−39.360 710[1]	−37.208 019[1]	−36.790 507	14.76	
14A	C_{2v}	46	4.373	**−56.754 744**	−44.827 522[1]	−41.717 043[1]			3.12
14B	C_{3v}	45	2.425	−56.660 471	**−45.619 277**	**−42.675 222**	−40.259 823	3.12	13.07
14C	C_{2v}	41	0.141	−55.971 62[2]	−43.634 048[1]	−41.249 282	**−40.798 348**	13.07	
15A	D_{6d}	50	9.527	**−63.162 119**	−47.570 579	−40.569 211[10]	−35.758 904[13]		3.74
15B	C_{2v}	49	2.573	−62.593 904	**−49.748 409**	**−46.541 404**	−44.086 633	3.74	12.71
15C	C_{2v}	45	0.141	−62.631 372[2]	−47.952 559	−45.293 844	**−44.806 437**	12.71	
16A	D_{3h}	54	11.222	**−69.140 648**	−50.834 213	−42.887 569[12]			3.41
16B	C_s	53	2.868	−68.757 203	**−53.845 835**	**−50.261 947**	−47.831 957	3.41	11.99
16C	C_{2v}	49	0.142	−68.575 718[1]	−52.265 348	−49.338 173	**−48.814 517**	11.99	
17A	D_{3h}	58		**−75.662 417**	−53.156 042[2]				3.41
17B	C_{3v}	57	3.372	−75.147 372	−57.884 517	−53.772 213	−51.329 560	3.41	4.88
17C	C_s	57	3.281	−75.091 367	−57.912 963	−53.862 044	−51.440 588	4.88	4.91
17D	C_2	57	3.163	−75.005 403	**−57.941 386**	**−53.983 559**		4.91	11.31
17E	C_{2v}	53	0.142	−74.868 92[1]	−56.573 571	−53.382 277	**−52.822 588**	11.31	
18A	C_2	65		**−82.579 266**	−59.881 449[1]			2.18	3.03
18B	C_{5v}	62	4.500	−82.548 885	**−62.689 245**	**−57.657 135**	−54.059 707	3.03	10.35
18C	D_{5h}	57	0.142	−81.490 185	−60.926 500	−57.429 683	**−56.830 907**	10.35	
19A	D_{5h}	68	6.001	**−90.647 461**	**−68.492 285**	**−62.166 843**	−56.676 685		10.70
19B	C_{2v}	61	0.151	−87.485 744	−65.064 771	−61.427 105	**−60.812 425**	10.70	
20A	C_2	73		−96.954 554[1]	−69.674 303[1]				2.02
20B	C_{2v}	72	6.507	**−97.417 393**	**−72.507 782**	**−65.679 115**	−61.327 229	2.02	10.24
20C	C_{2v}	65	0.162	−94.222 416	−69.202 704	−65.423 697	**−64.791 953**	10.24	
21A	C_{2v}	76	7.133	**−104.336 946**	−76.487 266	−69.068 687	−65.179 591[1]		5.39
21B	C_1	76	6.922	−104.004 129	**−76.529 139**	−69.276 346	−65.778 898	5.39	9.87
21C	C_{2v}	69	0.178		−73.345 300	**−69.415 060**	**−68.760 669**	9.87	
22A	C_s	81	8.198	**−112.041 223**	**−81.136 735**	−73.014 321	−68.580 862[1]		9.68
22B	C_{2v}	73	0.204	−106.637 295[1]	−77.492 169	**−73.397 282**	**−72.711 122**	9.68	
23A	D_{3h}	87	10.597	**−120.786 879**	**−86.735 494**	−76.630 624	−70.816 059[5]		9.58
23B	D_{5h}	77	0.237	−111.961 860	−81.637 940	**−77.372 686**	**−76.647 340**	9.58	
24A	C_{3v}	94	16.499	−127.617 205	−88.449 980[2]	−77.726 337[2]		2.09	2.79
24B	C_s	91	10.947	**−127.884 549**	**−90.685 398**	−80.295 459[1]	−74.613 738[2]	2.79	8.61
24C	C_{2v}	84	2.979		−88.588 397	**−81.694 952**	−78.332 810	8.61	11.49
24D	C_s	80	0.005	−119.576 180	−85.629 390	−80.774 615	**−80.133 387**	11.49	
25A	C_{3v}	102	19.496	−135.605 043	−92.440 314	−82.733 432[1]	−92.440 314[2]		2.62
25B	C_s	96	12.090	**−136.072 704**	**−95.127 899**	−84.168 765		2.62	8.27
25C	C_1	88	2.982		−93.056 563	**−85.754 661**	−82.341 324	8.27	10.05
25D	C_{2v}	85	0.225	−131.870 633[2]	−91.756 110	−85.732 161	**−84.742 334**	10.05	

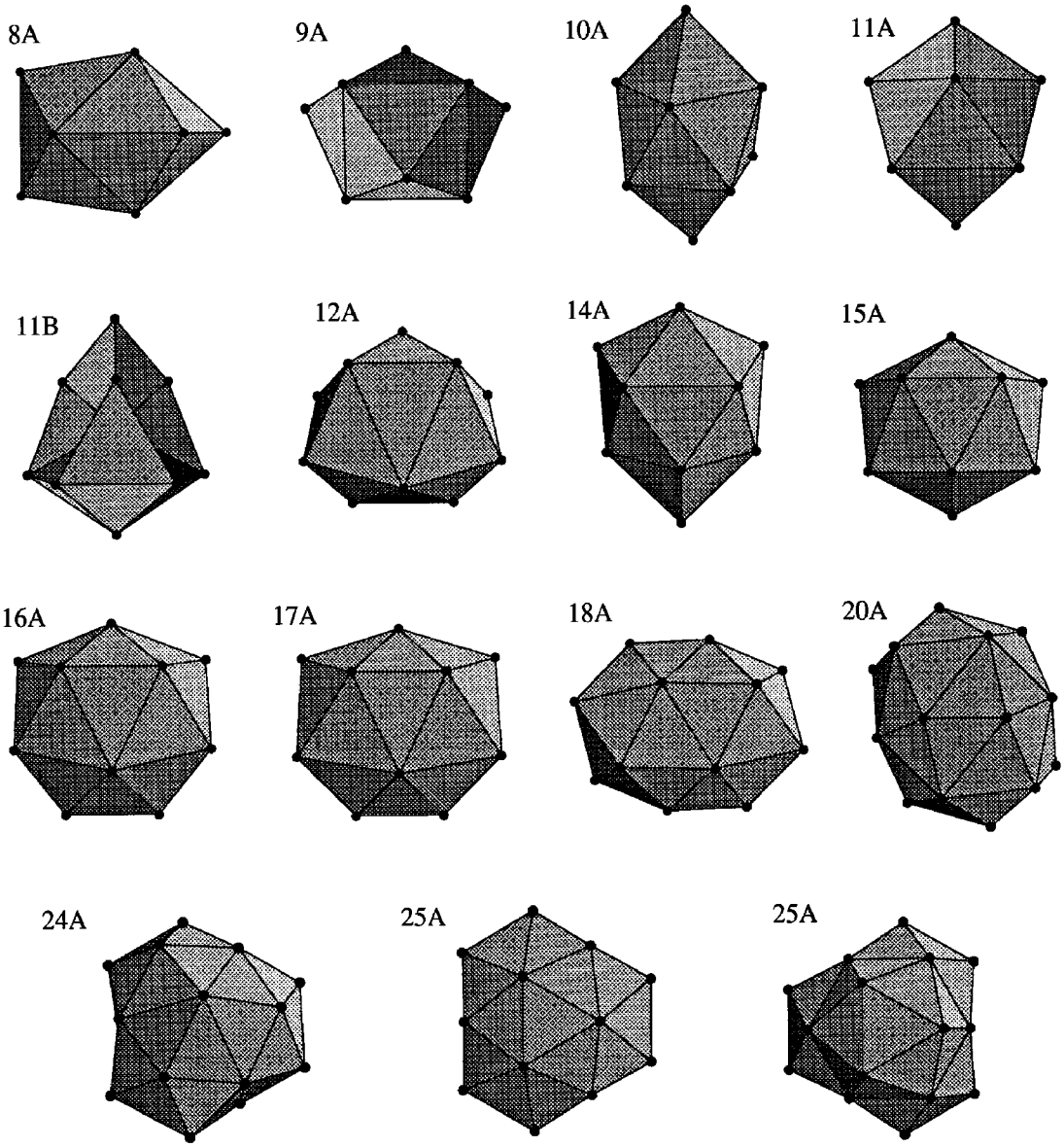

FIG. 2. Global minima associated with low values of ρ_0. Each structure is labeled by the symbol given in Table I. The graphics were produced with MATHEMATICA[45] using a cutoff of 1.2 for triangulation.

mally coordinated, and have an energy equal to the lower bound $-N(N-1)/2$. As shown by Braier *et al.*,[7] the octahedron and the pentagonal bipyramid are always the global minimum for M_6 and M_7. M_8 is the first cluster for which we found the global minimum to change as a function of the range, and similar transitions occur for all larger clusters. It is our aim here not only to identify all these changes in the global minimum, but to explain them in terms of the analysis given in Sec. II A, and to gain from them a comprehensive understanding of the effects of the range of the potential on cluster structure.

In Table I we give all the minima we found for M_5–M_{25}, which are global minima for some range of ρ_0, together with their point groups, energies, and the range of ρ_0 for which they are the global minimum ($\rho_{\min}$ and $\rho_{\max}$ are the bounds of this range). We have divided the global minima found into four main structural classes: icosahedral, decahedral, close-packed, and structures associated with low ρ_0. The global minima are depicted in Figs. 2–5, in accordance with this classification.

The group of structures associated with low ρ_0 are close to spherical in shape and in the main are highly strained in order to maximize n_{nn}. The exceptions are 8A, 9A, and 10A (Fig. 2). These clusters have smaller values of n_{nn} than their ''rival'' minima, which are based upon incomplete centered icosahedra, but have a lower energy because of a larger contribution from E_{nnn}; the next-nearest-neighbor shell is significantly closer than for the icosahedra. In each case the structures are roughly spherical but do not have an atom in the center of the cluster. As can be seen from Table I, for $N \geqslant 11$ the global minimum at low ρ_0 is the most strained global minimum for that cluster size. Structure 11A is the same as 10A, but with an atom in the center of the cluster—it is a centered bicapped square antiprism. Encapsulation of the central atom leads to considerable strain, which is manifested as surface tension. For 14A, the central atom is surrounded

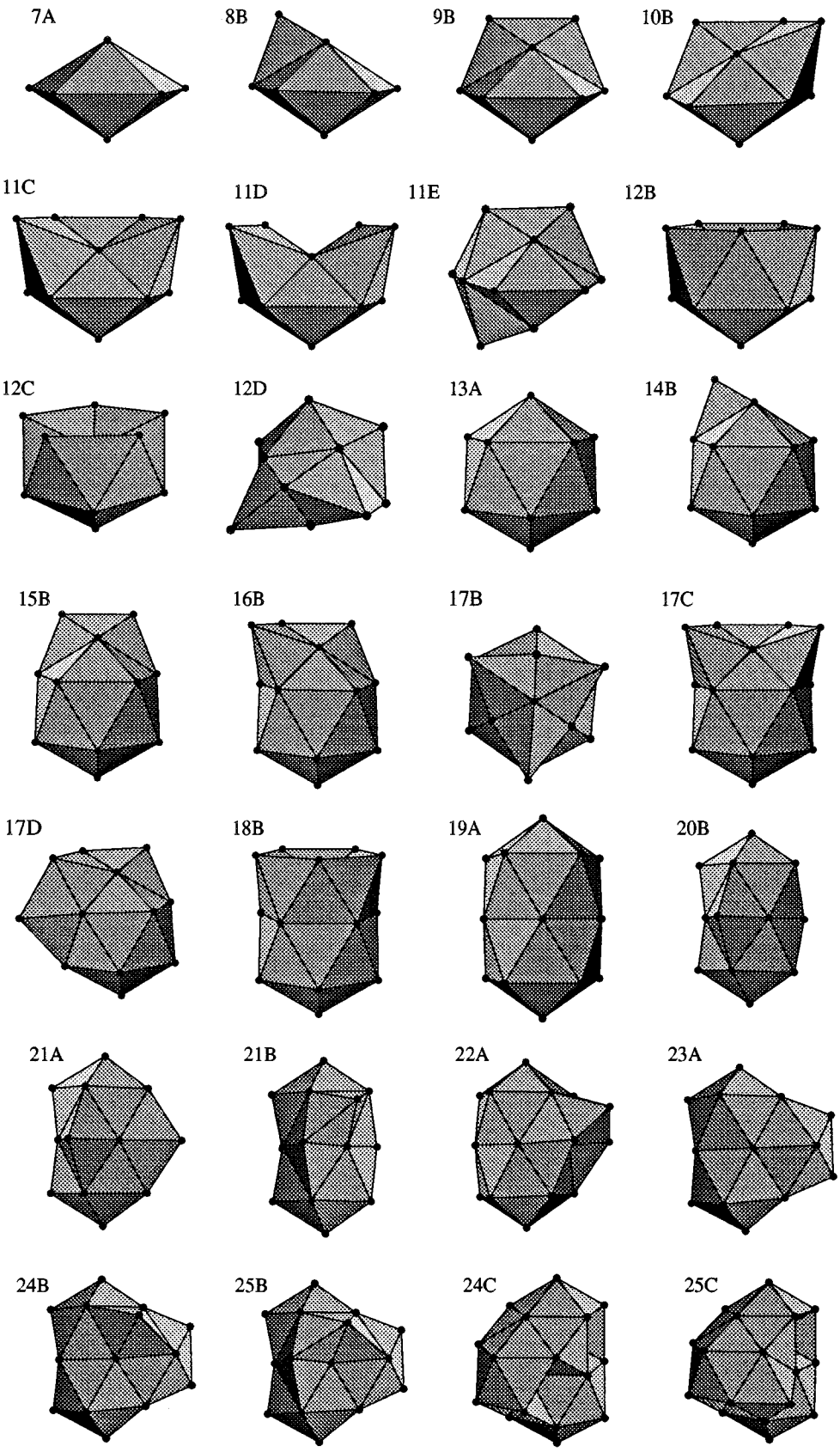

FIG. 3. Global minima based on icosahedral packing.

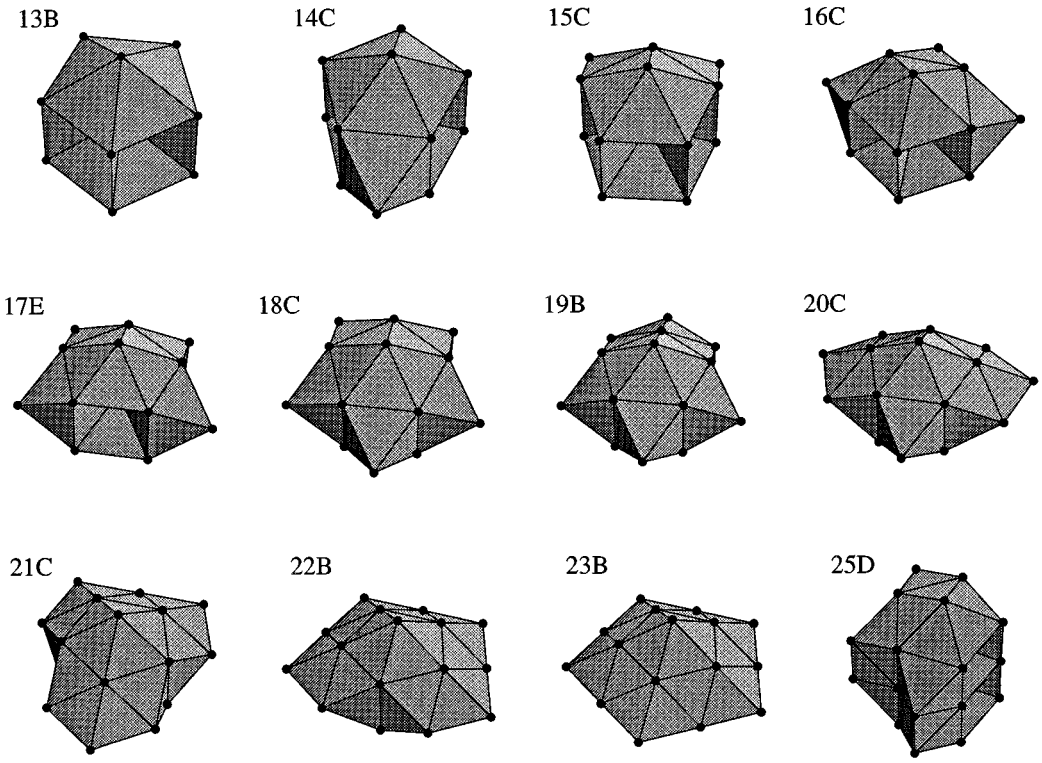

FIG. 4. Global minima based on decahedral packing.

by 13 atoms, and so the surface is now in compression. The first cluster to have two atoms in the center is 17A. It is the same as 16A, but with two enclosed atoms on the threefold axis. All the above-mentioned clusters are illustrated in Fig. 2. This structural class does not have a common lattice, or packing scheme, which makes prediction of low-energy structures at low ρ_0 far from easy.

The structures we have found at low ρ_0 are very similar to some of those reported by Stave and DePristo in their studies of nickel and palladium clusters.[17] The lowest-energy structures they found are the same as our 5A, 6A, 7A, 8A, 9A, 10B, 11C, 12B, 13A, 14A, 15A, and 16A. The range of the potential must be one of the crucial factors in determining the structure in clusters of these two metals.

Icosahedral clusters are the most stable structures for the LJ potential, and exactly the same series of clusters is the most stable for the Morse potential with $\rho_0=6$. For $N<13$ these clusters are incomplete icosahedra. This series of structures resembles those adopted by borohydrides,[46] although the borohydrides have no central atom. As ρ_0 increases the incomplete icosahedra are destabilized because of their strain energy. For M_{11} and M_{12} structures based on incomplete icosahedra, but with one or two nearest-neighbor contacts broken (11D and 12C), first become lower in energy. This symmetry breaking allows the other nearest-neighbor contacts to relax closer to the pair equilibrium distance and so reduce the strain. At still larger ρ_0, structures with a different capping sequence of the pentagonal bipyramid (11E and 12D) become more stable, again because they have lower strain. They are both fragments of the 19-atom double icosahedron. In the Hoare and Pal's classification, they would be called polytetrahedral.[47]

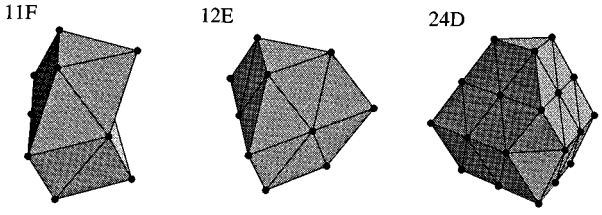

FIG. 5. Global minima based on close-packing.

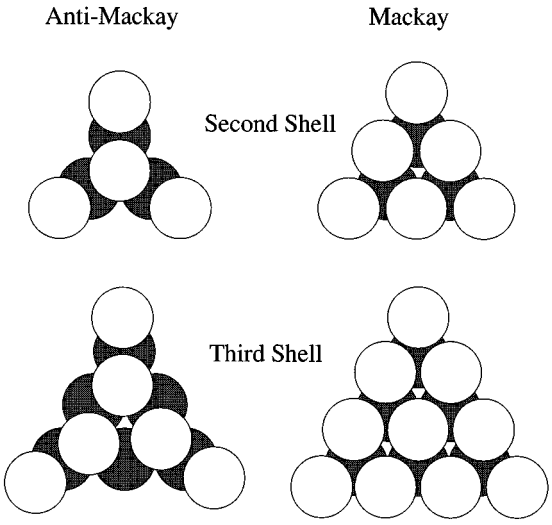

FIG. 6. Atomic positions for the two possible overlayers of the icosahedron, anti-Mackay (left), and Mackay (right). These are shown for a single face of the icosahedron.

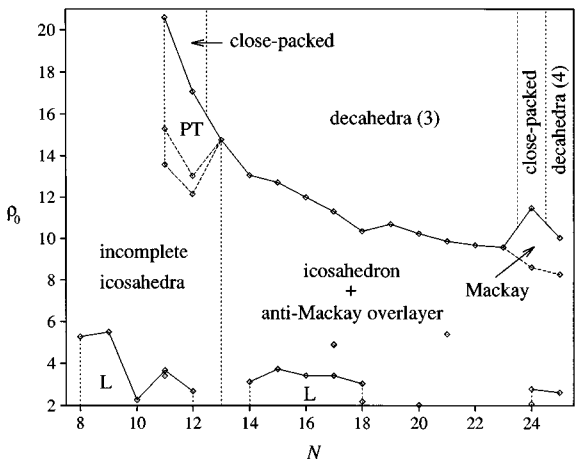

FIG. 7. ''Phase diagram'' showing the variation of the lowest-energy structures with N and ρ_0. The data points are the values of ρ_0 for which the global minimum changes. PT denotes polytetrahedral structures and L structures associated with low ρ_0. The decahedral structures are labeled by the number of atoms along the five-fold axis.

For $N>13$, there are two possible sites that the atoms can occupy on the surface of the cluster. These two possibilities are illustrated in Fig. 6. The anti-Mackay overlayer leads to the 45-atom rhombic tricontahedron with I_h point group symmetry,[48] and the Mackay overlayer leads to the 55-atom Mackay icosahedron.[49] The Mackay sites continue the fcc close-packing that exists in each of the 20 distorted tetrahedra from which the icosahedron is constructed. In previous studies, the anti-Mackay overlayer has been referred to as polyicosahedral,[50] because the growth sequence includes structures with interpenetrating icosahedra, such as the double (19A) and triple (23A) icosahedra. It has also been called the face-capping overlayer.[29]

For LJ clusters, the anti-Mackay overlayer is initially filled, but for $N\geqslant 31$ the Mackay overlayer is more stable.[29] The anti-Mackay overlayer has a greater n_{nn} than clusters of the same size with the Mackay overlayer, but it also has greater E_{strain}. Consequently, decreasing the range of the potential destabilizes the anti-Mackay overlayer with respect to the Mackay overlayer. This effect is seen for M_{24} and M_{25}, where clusters with the Mackay overlayer are most stable for $\rho_0=10$. It is expected that the value of ρ_0 for which the global minimum changes from anti-Mackay to Mackay decreases as the size increases, because the strain associated with the anti-Mackay overlayer progressively increases. The start of this trend is seen for M_{24} and M_{25} in Fig. 7. For $\rho_0=6$ it is expected that the Mackay overlayer is more stable for $N\geqslant 31$, as for the LJ potential. For potentials with a longer range, this crossover will occur at a larger size. This effect has been seen in *ab initio* molecular dynamics calculations of lithium clusters,[51] where the anti-Mackay overlayer is lowest in energy up to $N=45$.

For M_{17} and M_{22}, there is more than one icosahedral-based structure with the same highest value of n_{nn}. The precise strains determine which isomer is the global minimum at a particular value of ρ_0. From $N=13$ to $N=23$, we find a series of structures based on decahedra with three atoms along the five-fold axis. 23B, the decahedron (or pentagonal bipyramid) is the completion of this sequence. The lowest-energy decahedral clusters for larger N are not based on adding another shell to this decahedron, but instead a sequence of incomplete decahedra with four atoms along the five-fold axis is more stable. As can be seen in Fig. 7 the value of ρ_0 for which the decahedral clusters become more stable than the anti-Mackay icosahedral sequence decreases with N because of the increasing strain energy of the icosahedral clusters.

M_{11}, M_{12}, and M_{24} are the only clusters for which close-packed structures are global minima. This is probably because for M_{11} and M_{12} there are no low-energy decahedral clusters, and at $N=24$ the decahedral sequence changes. Low-energy close-packed structures exist for most other sizes at large ρ_0, but they never appear to become the global minimum for the values of ρ_0 we consider here.

The lowest-energy structures at $\rho_0=13.6$ are likely to be the global minima for C_{60} clusters modeled by the Girifalco potential.[31] For example, reoptimization of the coordinates of 19B for the Girifalco potential gave a structure with an energy of $-62.693\,166\epsilon$ (where the equilibrium pair well depth for the Girifalco potential, ϵ, is 3218.43 K), which is significantly lower than any previously reported[26] for $(C_{60})_{19}$.

To analyze which values of N might be ''magic number'' clusters for potentials with different ranges, we calculated the second finite difference of the energy, $\Delta_2 E=E(N+1)+E(N-1)-2E(N)$ as a function of ρ_0. These are shown in Fig. 8. Peaks in $\Delta_2 E$ correspond to especially stable clusters. For $\rho_0=6$, the pattern is the same as for the LJ potential, with magic numbers at $N=7$, 10, 13, 19, and 23. The last three values correspond to the single, double, and triple icosahedron, respectively. For smaller ρ_0 the peaks at $N=7$ and 10 disappear, and at larger ρ_0 the magic number character of the icosahedra diminishes. For $\rho_0=14$, the small peak at $N=23$ instead corresponds to the complete decahedron. The pattern for $\rho_0=14$ is likely to be very similar to that for C_{60} clusters, but it differs markedly from the results of Rey *et al.*[28] The latter authors probably did not find the global minima, but we could not check this hypothesis because they did not report the energies or structures of their lowest-energy clusters.

B. M_{38}, M_{46}, M_{55}, M_{70}, M_{75}, and M_{79}

A small selection of larger clusters was also studied. Mapping the PES for these systems is obviously much more demanding than for the clusters in the previous section. M_{38}, M_{55}, M_{75}, and M_{79} were chosen because they have especially stable fcc-, icosahedral-, decahedral-, and fcc-based structures, respectively. M_{46} and M_{70} should be representative of nonmagic number clusters. In Table II we describe the global minima that we found for these five sizes, and their structures are depicted in Figs. 9–11 and 13–15.

Structures 38B and 38C are icosahedral clusters with an anti-Mackay overlayer and are the most stable for low ρ_0. They both have two face-capping atoms and five vertex-capping atoms missing from the complete overlayer, and only differ in the position of the fifth vertex hole. At very low ρ_0, structure 38A becomes more stable. It is similar to structures 38B and 38C, but is considerably distorted, pro-

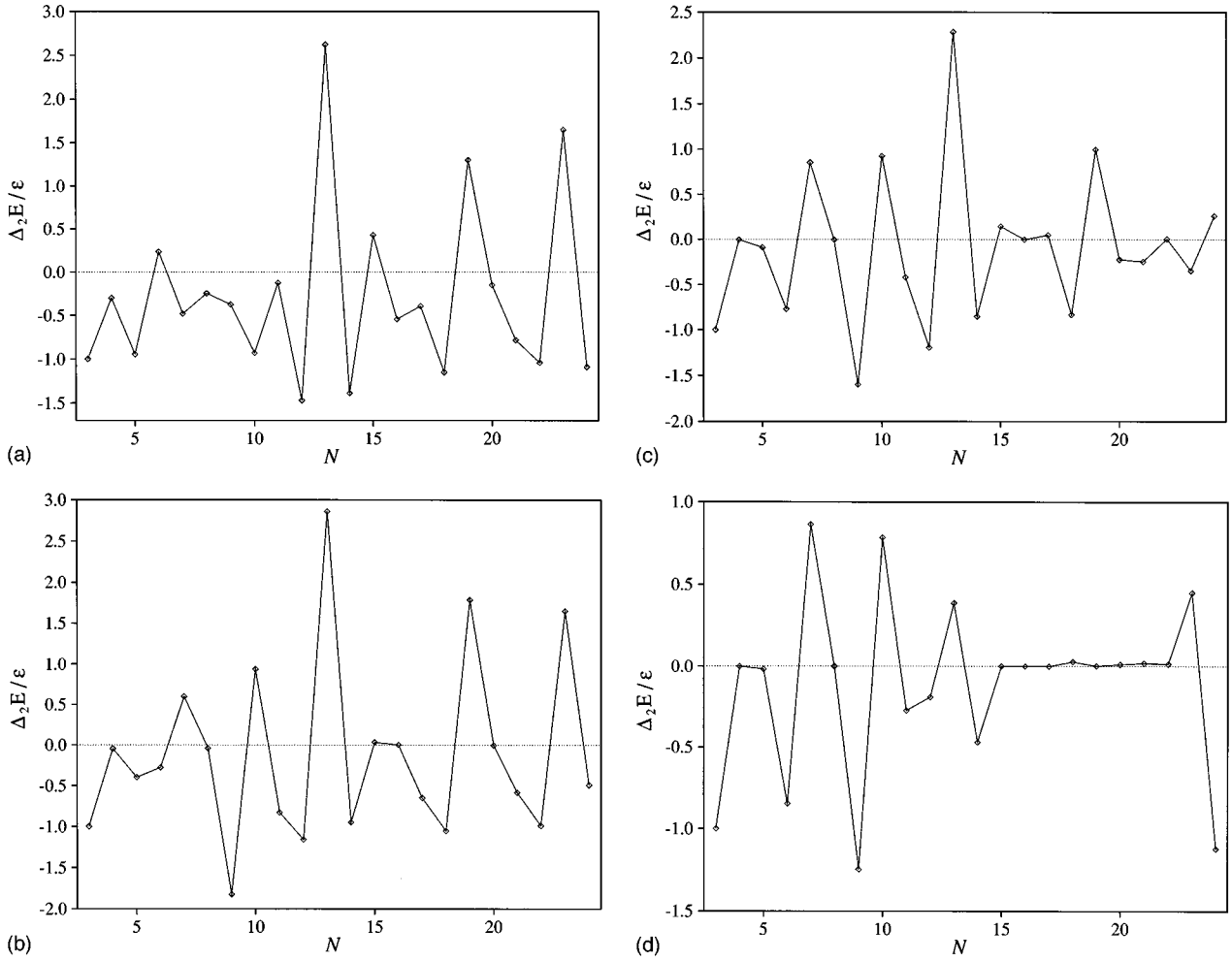

FIG. 8. Plots of $\Delta_2 E$ as a function of N for (a) $\rho_0=3$, (b) $\rho_0=6$, (c) $\rho_0=10$, and (d) $\rho_0=14$.

ducing a more spherical shape. As expected, icosahedral clusters with a Mackay overlayer become more stable for a shorter-ranged potential ($\rho_0>4.83$). However, they are never the global minimum, because an fcc truncated octahedral structure, 38D, is always more stable. Decahedral structures are also never the global minimum; the lowest-energy decahedral minimum has one less nearest-neighbor contact than 38D. The truncated octahedron is also the most stable structure for the Lennard-Jones potential, with an energy of $-173.928\,427\epsilon$, 0.79ϵ lower than the lowest-energy icosahedral cluster found by Northby.[29] The 38-atom LJ cluster is the smallest size with an fcc global minimum. This is particularly interesting as the the crossover from the decahedral to fcc morphology, predicted on the basis of the most stable sequence[4] is at $N\approx 10^5$. These two results are not in contradiction, but instead show that comparisons of magic number sequences provide only a general guide for predicting the type of structure that will be most stable at a particular N.

38D's special stability—it is the global minimum for a large range of ρ_0 and has the lowest value of $\rho_{\min}$ found for the fcc clusters considered in this study—can be understood from both the Wulff construction[52] and the analysis of Sec. II A. The Wulff construction can be used to predict the most stable morphology of macroscopic crystals if the surface energies of the facets are known, and has also been found to be useful for predicting especially stable sequences of clusters.[53] If only nearest-neighbor contacts are considered in calculating the surface energies (or equivalently $\rho_0\rightarrow\infty$), the Wulff polyhedron for fcc crystals is the truncated octahedron with regular hexagonal faces.[53] This shape maximizes the number of nearest-neighbors for fcc clusters. 38D belongs to this sequence of structures ($N=38,201,586,...$), which is likely to be the most stable fcc sequence for short-ranged potentials, such as that appropriate for C_{60}. For longer-ranged potentials, further faceting of the Wulff polyhedron occurs, giving it a more rounded shape.[54] Recently, there has been some experimental evidence that small clusters may adopt the structure of 38D. EXAFS (extended x-ray absorption fine structure) spectra of small gold clusters have been interpreted as providing evidence for truncated octahedral clusters, and particularly for the 38-atom truncated octahedron.[55]

Structure 46A is based on the complete 45-atom rhombic tricontahedron. The extra atom does not go into a new shell, but is accommodated in the existing outer shell. Figure 10 gives a view of 46A, which shows the distortion from fivefold symmetry caused by this extra atom. Structure 46B is an incomplete Mackay icosahedron. Two complete triangular faces of the icosahedron are missing. It is the lowest-energy minimum found for the LJ potential.[29] 46C and 46D are a

TABLE II. Minima for M_{38}, M_{46}, M_{55}, M_{70}, M_{75}, and M_{79}. Energies at values of ρ_0 for which the structure is lowest in energy are given in bold. $\rho_{\min}$ and $\rho_{\max}$ give the range of ρ_0 for which the minimum is lowest in energy. For 55E, 55F, and 55G no values are given because they are never the global minimum. If at a particular value of ρ_0 a structure is not a minimum, but a higher-order saddle point, the index of the stationary point is given in square brackets after the energy. E_{strain} has been calculated at $\rho_0=10$. If a structure is not stable at $\rho_0=10$ no value of E_{strain} is given. All energies are given in ϵ.

	Point group	n_{nn}	E_{strain}	$\rho_0=3.0$	$\rho_0=6.0$	$\rho_0=10.0$	$\rho_0=14.0$	$\rho_{\min}$	$\rho_{\max}$
38A	D_2	164	30.138	**−249.159 174**	−153.208 710[3]	−134.319 674[3]			3.05
38B	C_1	163	27.962	−249.087 740	−154.165 069	−135.519 468	−129.339 213	3.05	4.70
38C	C_s	163		−248.600 369	−154.041 575			4.70	4.76
38D	O_h	144	0.013	−246.414 723[4]	**−157.406 902**	**−145.849 817**	**−144.321 054**	4.76	
46A	C_s	207		**−327.033 118**					3.96
46B	C_{2v}	186	6.646	−320.118 738[1]	**−199.177 751**	**−181.236 182**	−174.605 103[1]	3.96	10.46
46C	C_s	179	0.452		−194.923 850	−180.711 434	−178.517 769	10.46	11.81
46D	C_s	179	0.451		−194.876 995	−180.708 654	**−178.519 320**	11.81	15.08
46E	C_1	178	0.017	−323.212 794	−194.507 423	−180.244 056	−178.386 833	15.08	
55A	C_1	252		**−417.918 562**					3.52
55B	I_h	234	10.543	−416.625 645	**−250.286 609**	**−225.814 286**	−213.523 774	3.52	11.15
55C	C_{2v}	221	0.465		−242.622 450	−223.482 018	**−220.646 208**	11.15	21.83
55D	C_{3v}	219	0.026		−241.679 658	−222.082 489	−219.532 333	21.83	
55E	C_1	220	0.252		−241.722 520	−222.726 682	−220.070 631		
55F	D_{5h}	219	0.626		−241.407 941	−221.472 406	−218.356 911		
55G	O_h	216	0.029		−239.138 585[1]	−219.227 882	−216.564 472		
70A	C_1	332		**−577.286 914**	−313.362 561				3.69
70B	C_{5v}	304	15.324		**−325.887 749**	−291.872 039	−276.370 075	3.69	7.89
70C	C_s	293	0.676		−323.082 118	**−296.412 149**	**−292.439 398**	7.89	17.69
70D	C_{2v}	291	0.035		−321.447 249	−295.093 593	−291.706 484	17.69	
75A	C_s	359		**−633.298 200**					3.75
75B	C_1	328	18.559	−630.521 082	−351.177 041	−312.987 148	−296.598 914	3.75	5.82
75C	D_{5h}	319	0.718		**−351.472 365**	**−322.643 558**	**−318.407 330**	5.82	21.13
75D	C_{4v}	316	0.035		−348.840 841	−320.397 941	−316.757 605	21.13	
79A	C_1	385		**−678.940 231**	−358.579 695				3.18
79B	C_{2v}	348	19.381	−673.564 685	**−372.832 290**	−332.365 043		3.18	6.53
79C	C_{2v}	343	11.973		−372.465 768	−335.139 012	−320.222 688	6.53	6.67
79D	C_{2v}	337	0.783	−663.444 178	−371.568 226	**−340.862 137**	−336.332 369	6.67	11.49
79E	O_h	336	0.036		−370.783 965	−340.631 754	**−336.796 220**	11.49	

continuation of the decahedral sequence started with 24A. Completion of this sequence would lead to the 54-atom decahedron. However, at some point before this sequence terminates, incomplete decahedra with five atoms along the fivefold axis become more stable. Structure 46E is based on the 31-atom truncated tetrahedron. Two of the faces have been covered by hexagonal overlayers. These atoms do not occupy fcc-type sites, but the alternative hcp-type sites. The additional atom occupies a four-coordinate site. As ρ_0 is increased for M_{46}, we see the crossovers from icosahedral to decahedral to fcc structures that we anticipated in Sec. II A.

As the 55-atom cluster is a magic number species for various atomic[37,56–59] and molecular systems,[57,60] it has often been investigated. It is the second cluster in the magic number sequence $N=13$, 55, 147, 309,... . The structures normally considered in an analysis of the 55-atom PES are the high symmetry icosahedron (55B), Ino's truncated decahedron[61] (55F) and the fcc cuboctahedron (55G). Studies of the size dependence of cluster structure often compare these three isomeric sequences.[3,62–64] However, for many systems this is not a good comparison, as the truncated deca-

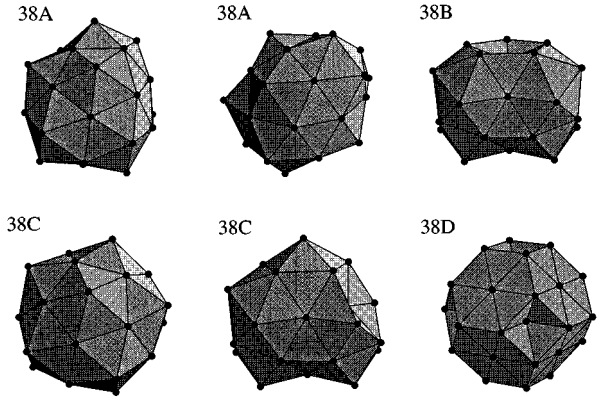

FIG. 9. Lowest-energy minima found for M_{38}.

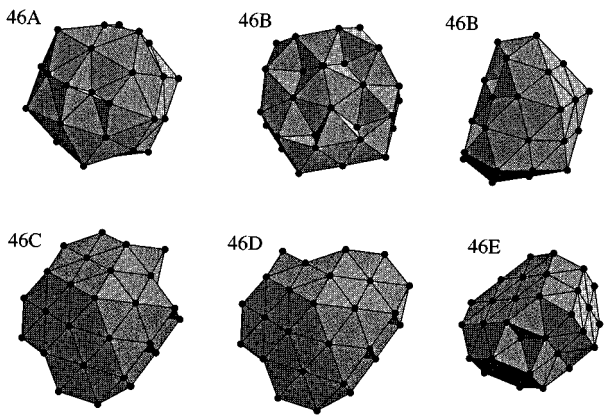

FIG. 10. Lowest-energy minima found for M_{46}.

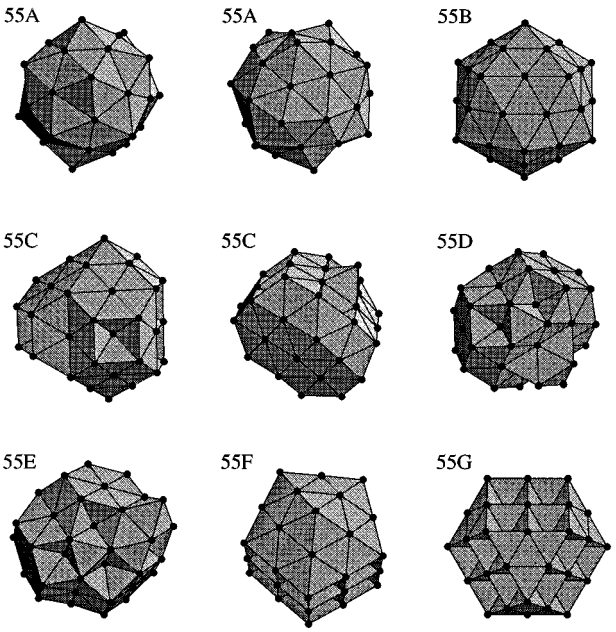

FIG. 11. Lowest-energy minima found for M_{55}.

hedron and cuboctahedron do not represent the optimal sequences of decahedral and fcc structures. This is because they have a significant proportion of atoms on high-energy {100} faces, and consequently they have low values of n_{nn}. Marks noted that a more stable decahedral sequence could be formed, which has reentrant {111} faces between the edges of the {100} faces.[65] For fcc LJ clusters, a sequence based on the truncated octahedron is more stable,[2] and even lower-energy sequences have been found by Raoult *et al.*, which involve further faceting.[4]

Furthermore, in this study we have found that the decahedron and the cuboctahedron are *never* the lowest-energy decahedral or fcc 55-atom clusters. We found four global minima in the range of ρ_0 we considered. They are depicted in Fig. 11 and the low-lying minima based on these structures are given in Tables III–VI. 55C and 55E represent the optimal 55-atom decahedral and fcc structures, respectively. It can be seen from Fig. 12 that the decahedron and cuboctahedron are significantly higher in energy than 55C and 55E for all values of ρ_0. Both 55C and 55E have a significantly higher proportion of {111} faces, and therefore a larger n_{nn}. 55C is obtained from Ino's decahedron[61] by removing one square face and redistributing these nine atoms. Eight are placed on the two intact square faces in sites, corresponding to the third shell of the decahedron. The other atom can cap any one of the four types of exposed four-coordinate sites to give four minima with very similar energies (Table V). In the lowest-energy minimum the atom occupies the central site of the missing square face. 55C can also be viewed as an incomplete 75-atom Marks' decahedron. The other low-lying minima given in Table V have a surface defect and an extra capping atom. For the Girifalco potential[31] 55C has an energy of $-231.073\,017\epsilon$, lower than any previously reported[26] structure for $(C_{60})_{55}$.

As for M_{46}, the lowest-energy M_{55} fcc clusters are based on the 31-atom truncated tetrahedron. Three of its faces are covered by hexagonal overlayers, leaving three atoms that can occupy various sites (Table VI). For 55E, the lowest-energy fcc isomer for most values of ρ_0, these three atoms bridge one of the grooves between hexagonal overlayers. The beginnings of a five-fold axis can be seen along this groove. This illustrates the fact that the structure of a decahedron is based on five twinned tetrahedra, and suggests a possible mechanism for transformation between decahedral and fcc structures. For 55D, the global minimum at very large ρ_0, the three atoms start to form an overlayer on the fourth face of the tetrahedron.

As for the LJ potential, the icosahedron is the lowest-energy structure for $\rho_0=6$. Reflecting its magic number character, it is the global minimum for a wide range of ρ_0, and there is a large energy gap between it and the next lowest-

TABLE IV. The ten lowest-energy minima found for M_{55} based on the icosahedron, 55B, at $\rho_0=6$.

Energy/ϵ	Point group	n_{nn}
−250.286 609	I_h	234
−247.696 784	C_s	231
−247.695 826	C_s	231
−247.694 117	C_s	231
−247.539 674	C_1	231
−247.458 479	C_s	231
−247.457 474	C_s	231
−247.455 468	C_1	231
−247.455 258	C_1	231
−247.453 356	C_1	231

TABLE III. The ten lowest-energy minima found for M_{55} at $\rho_0=3$.

Energy/ϵ	Point group	n_{nn}
−417.918 562	C_1	252
−417.702 577	C_s	249
−417.685 608	C_2	256
−417.633 629	C_s	248
−417.504 209	C_s	252
−417.489 770	C_{2v}	258
−417.444 435	C_1	252
−417.374 002	C_1	252
−417.347 120	C_s	252
−417.325 958	C_1	252

TABLE V. The ten lowest-energy decahedral minima found for M_{55} based on 55C at $\rho_0=14$.

Energy/ϵ	Point group	n_{nn}
−220.646 208	C_{2v}	221
−220.645 856	C_s	221
−220.644 370	C_1	221
−220.643 600	C_s	221
−219.789 384	C_1	220
−219.785 611	C_1	220
−219.781 762	C_1	220
−219.685 715	C_1	220
−219.675 778	C_1	220
−219.674 931	C_1	220

TABLE VI. The ten lowest-energy fcc minima found for M_{55} at $\rho_0=14$.

Energy/ϵ	Point group	n_{nn}
−220.070 631	C_1	220
−220.069 086	C_1	220
−220.068 764	C_1	220
−220.068 747	C_1	220
−220.068 569	C_s	220
−220.067 876	C_1	220
−219.789 483	C_1	220
−219.764 530	C_1	220
−219.532 333	C_{3v}	219
−219.496 445	C_{3v}	219

energy minimum (Table IV). These low-lying minima have a surface defect at a vertex site and a single capping atom. Of these minima, the four lowest in energy have the cap in the center of one of the triangular {111} faces, and for the others the cap is in an off-center site.[66]

At low ρ_0, other more strained minima become lower in energy than the icosahedron. At these very long ranges, the PES becomes smoother and flatter. There are many low energy minima (Table III) with small barriers between them. In fact, there are at least 86 minima within 2ϵ of 55A. In places, the surfaces of these clusters exhibit the characteristic fivefold coordination of the complete anti-Mackay overlayer (as in the first view of 55A in Fig. 11), but in other places there is no discernible order (as in the second view). The disorder in these clusters is a direct result of the increase in the range of the potential. The tolerance of strain leads to the breakdown of regular packing. The differentiation between nearest-neighbor and next-nearest-neighbor becomes ambiguous and the method of determining n_{nn} somewhat arbitrary. For these clusters, we choose to define n_{nn} as the number of contacts that have an energy lower than -0.6ϵ, 60% of the equilibrium pair well depth, at $\rho_0=4.0$. The core of structure 55A is not the 13 atom icosahedron, but instead structure 15A. Some of the low-energy minima given in Table III have 14A or 16A at their core. These structures have many similarities to the liquid-like inherent structures[38] found for larger ρ_0 when the Mackay icosahedron melts. Both types of structure involve a mixture of disorder and local icosahedral order, have a diffuse radial distribution function, and are strained. The energies of these minima correlate with the liquid-like minima when reoptimized at larger values of ρ_0. This relationship will be explored elsewhere in a study of the phase behavior of M_{55} and the effect of the range of the potential on the stability of the liquid-like state.[67]

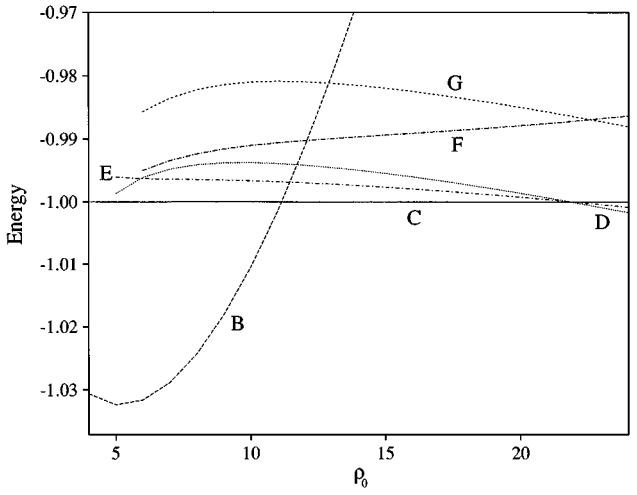

FIG. 12. Plot of the energies of structures 55A–G as a function of ρ_0. The binding energy of 55C has been used as the unit of energy. Each line is labeled by the letter of the appropriate structure.

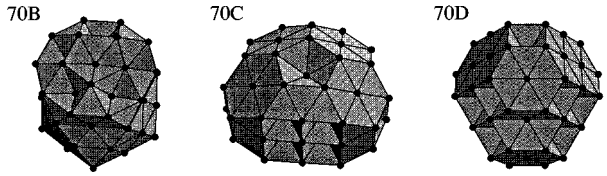

FIG. 13. Lowest-energy minima found for M_{70}.

The icosahedral, decahedral, and fcc structures for M_{70}, M_{75}, and M_{79} are very similar. The icosahedral clusters are based on the 55-atom icosahedron, with part of the anti-Mackay overlayer filled. 70B (Fig. 13) and 79B (Fig. 15) are the same as the lowest-energy structures found by Northby for the LJ potential.[29] However, 75B (Fig. 14) is lower in energy than the structure found by Northby for both the Morse and LJ potential. Its energy when reoptimized for the LJ potential is $-396.282\,249\epsilon$, approximately 0.25ϵ lower in energy than the Northby minimum. It includes an atom capping part of the incomplete third shell, a possibility that Northby did not consider.

For the LJ potential, the anti-Mackay overlayer is always lowest in energy for $N\leqslant 76$, and the Mackay overlayer for $N\geqslant 86$. In between these ranges, both overlayers have similar energies,[29] and the identity of the lowest varies with N. For the sizes we have considered, 79C (Fig. 15) is the only structure with a Mackay overlayer that becomes lowest in energy, and this is only true for a very small range of ρ_0. As for the smaller clusters, it is expected that the values of ρ_0 for the crossover between anti-Mackay and Mackay overlayers decreases as the size increases, and is always lower than 6 for $N\geqslant 86$.

The decahedral clusters are based on the Marks' decahedron, 75C. Structure 70C lacks one square overlayer and a vertex atom of the Marks' decahedron. For 79D, two of the grooves are filled to give larger {100} faces. The stability of the Marks' decahedron is seen from the range of ρ_0 for which 75C is the most stable structure (Table II). As is suggested by the lower limit ($\rho_{\min}=5.82$), 75C is also the lowest-energy

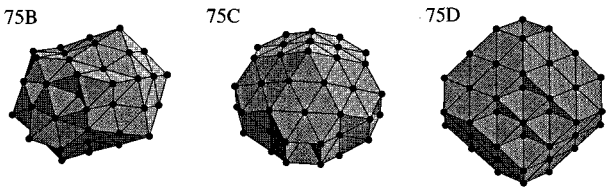

FIG. 14. Lowest-energy minima found for M_{75}.

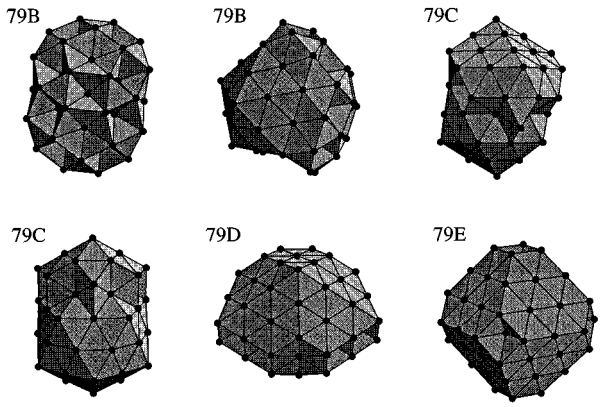

FIG. 15. Lowest-energy minima found for M_{79}.

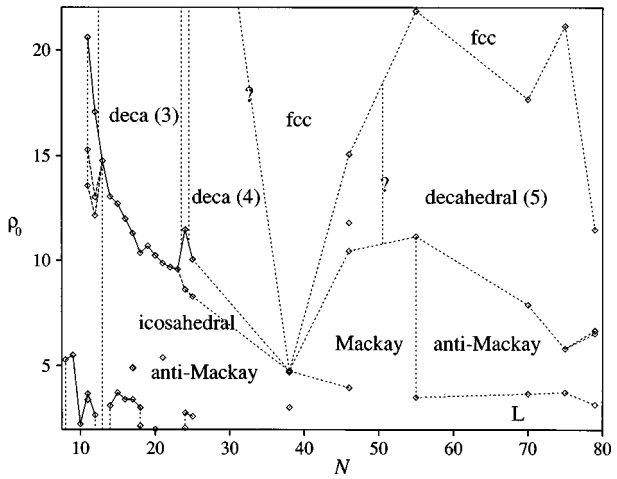

FIG. 16. ''Phase diagram'' for the lowest-energy structural type as a function of N and ρ_0. The data points are the values of ρ_0 for which the global minimum changes. L denotes structures associated with low ρ_0. The decahedral structures are labeled by the number of atoms along the five-fold axis. For larger N the boundaries have been estimated by interpolating between data points. It is expected that the real boundaries are a sensitive function of N. Question marks have been placed against the two estimated lines to make clear they are not based on any data points.

structure for the LJ potential; its energy is $-397.492\,331\epsilon$, 1.2ϵ lower than the lowest-energy 75-atom icosahedral LJ cluster. Similar decahedral structures are also lowest in energy for LJ_{76} and LJ_{77}, with energies of $-402.894\,866\epsilon$ and $-409.083\,517\epsilon$, respectively. For the LJ potential, the crossover from the icosahedral to the decahedral morphology based on the most stable sequence[4] is $N\approx1600$. However, as the most stable sequences for icosahedral and decahedral structures do not coincide in size, decahedral clusters may be lower in energy for a particular N below this figure.[4,68] The crossover at 75 atoms is particularly noteworthy.

The fcc clusters are based on the truncated octahedron, 79E (Fig. 15). The shape of this cluster is close to the Wulff polyhedron[52] and is formed from the cuboctahedron, 55G, by capping the six square {100} faces with a four-atom square overlayer. For 70D (Fig. 13), two of the cuboctahedron's faces are uncapped, and a vertex of the cuboctahedron has been removed. For 75D, one of the cuboctahedron's faces remains uncapped. Unlike the fcc clusters, 46E and 55D, these clusters have no twinning planes. The stability of the truncated octahedron is shown by its low value of $\rho_{\min}$, 11.49.

The most favorable structures associated with low ρ_0, 70A, 75A, and 79A show the same trends as 55A. These clusters are more disordered, but still have some anti-Mackay type surface structure. The complexity of the PES for these sizes, and the lack of a method of predicting low-energy structures for a very long-range potential, probably mean that, of all the potential global minima we have presented, it is most likely that these can be bettered.

Figure 16 gives an approximate ''phase diagram'' for the structure of the global minimum as a function of N and ρ_0. It has the form that we predicted in Sec. II A. At very long ranges, disordered structures not based on any type of lattice packing are most stable, at moderate ranges icosahedral structures are most stable, at short ranges decahedral structures are most stable, and at very short ranges fcc structures are most stable. The value of ρ_0 for a crossover between global minima is a sensitive function of N. In particular, large ranges of stability are found for the especially low-energy clusters, 38D, 55B, 75C, and 79E. However, there is an overall trend that the value of ρ_0 for the crossovers between icosahedral and decahedral structures, and between decahedral and fcc structures, decreases with N. This is because the strain energies increase more rapidly with N than the surface energies. Increasing the size destabilizes strained structures.

We cannot use Δ_2E as an indicator of magic numbers in this size range, as we did for the small clusters, because we have only considered a few examples. However, magic numbers are also expected if a structure is the global minimum for a wide range of ρ_0, and there is also a large-energy gap between this structure and the next lowest-energy isomer. These latter two conditions are satisfied by 38D, 55B, 75C, and 79E. For decahedral and fcc clusters, the magic numbers will probably be less pronounced, as the most stable sequences have a mixture of {111} and {100} faces. The decahedral sequence with only {111} faces is the decahedron itself, and for fcc there are two such sequences, the octahedron and the tetrahedron. These three sequences are not especially low in energy because of their nonspherical shape.

Our results are of particular relevance to studies of clusters of C_{60} molecules and the possibility of magic numbers. In a mass spectrometry experiment, Martin *et al.* probed the distribution of positively charged C_{60} clusters.[69] They found magic numbers at $N=13$, 55, and 147, which, combined with the intermediate peaks in the mass spectrum, indicated icosahedral structure. This study is not in disagreement with our results for a short-ranged Morse potential, because the positive charge modifies the intermolecular potential by introducing a longer-range Coulombic term. This, though, raises the questions, ''Do clusters of neutral C_{60} molecules exhibit magic numbers and, if so, at what sizes?'' For very small clusters, Δ_2E indicates possible magic numbers at $N=7$, 10, and 13. For the sizes we have considered with $N>13$, the global minima for the value of ρ_0 appropriate to C_{60} are mainly decahedral and sometimes fcc. Magic numbers are most likely for the lowest-energy sequences of structures.

TABLE VII. The ten lowest-energy decahedral minima found for M_{75} based on 75C at $\rho_0=6$.

Energy/ϵ	Point group	n_{nn}
−351.472 365	D_{5h}	319
−349.500 086	C_1	317
−349.498 552	C_1	317
−349.498 393	C_1	317
−349.496 058	C_1	317
−349.489 864	C_1	317
−349.275 647	C_1	317
−348.606 586	C_1	316
−348.332 763	C_1	316
−347.636 104	C_1	315

For decahedral packing, this is the sequence of Marks' decahedra at $N=75,192,389,\ldots$. For fcc packing, it is the sequence of truncated octahedra with regular hexagonal faces at $N=38,201,586,\ldots$, and a slightly higher-energy sequence with nonregular hexagonal faces at $N=79,140,314,\ldots$. Preliminary results from a study of larger Morse clusters[70] indicates that with $\rho_0=13.6$ the truncated octahedral sequence is lower in energy than the Marks decahedral sequence for $N>270$. This information suggests a scenario where decahedral magic numbers are dominant at small sizes, but with fcc magic numbers becoming more prominent as the size increases. Whether there might be an intermediate size range where both fcc and decahedral magic numbers might be observed due to the coexistence of the two structural types will depend on the thermodynamics and kinetics of the clusters in the molecular beam.

IV. DISCUSSION

In this paper we have attempted to find the global minimum for clusters as a function of ρ_0 and the number of atoms for the Morse potential. The global minimum represents the equilibrium structure at zero Kelvin. However, we need to ask the question, ''How important is the global minimum in determining the structure at a finite temperature?'' To answer this, we have to consider the contribution from other local minima on the PES. The thermodynamic properties of a collection of minima can be found by superposition of the density of states from each minimum. Such a method has been applied to LJ clusters using a harmonic approximation with reasonable success,[71,72] and when anharmonic corrections are included the results are very close to simulation.[41]

TABLE VIII. The ten lowest-energy icosahedral minima found for M_{75} based on 75B at $\rho_0=6$.

Energy/ϵ	Point group	n_{nn}
−351.177 041	C_1	328
−351.139 799	C_1	328
−351.135 122	C_s	328
−350.984 741	C_1	328
−350.912 649	C_1	328
−350.890 122	C_1	328
−350.874 153	C_1	328
−350.686 821	C_1	327
−350.612 539	C_s	329
−350.464 407	C_1	327

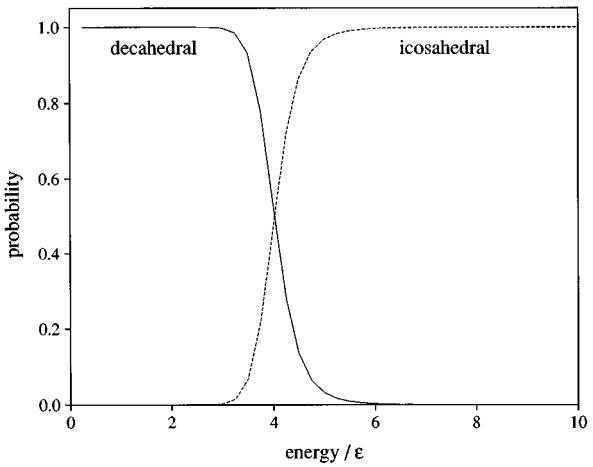

FIG. 17. Calculated equilibrium values for the microcanonical probability that an M_{75} cluster at $\rho_0=6$ has an icosahedral or a decahedral structure as a function of the total energy. The energy is measured with respect to the bottom of the well of the Marks' decahedron, 75C.

Here we apply this method to M_{75} at $\rho_0=6$ to illustrate the limitations of finite temperature structural predictions based on knowledge of the global minimum alone. For M_{75}, the Marks' decahedra, 75C, is the most stable cluster at $\rho_0=6$. There is an energy gap of 2ϵ to the next lowest-energy decahedral isomer (Table VII). At this value of ρ_0, the lowest-energy icosahedral structure is only 0.3ϵ higher in energy than 75C, and there are many icosahedral isomers of similar energy (Table VIII). In fact, we found 31 icosahedral isomers that were of lower energy than the second lowest-energy decahedral isomer. From this, it might be expected that as the energy is increased the density of states of the icosahedral isomers would become larger than the decahedral isomers, and so the structure would change from decahedral to icosahedral with increasing energy or temperature. This idea was tested using the harmonic superposition method. The total energy density of states, $\Omega(E)$, can be written as[71]

$$\Omega(E)=\sum_{E_s^0<E}\frac{n_s^*(E-E_s^0)^{\kappa-1}}{\Gamma(\kappa)\Pi_{j=1}^{\kappa}h\nu_j^s},$$

where the sum is over all known minima, $\kappa=3N-6$, E_s^0 is the potential energy of the minimum s, and n_s^* is the number of permutational isomers that is given by $n_s^*=2N!/h_s$, where h_s is the order of the point group of s. From this we can calculate p_i, the probability that a set of minima i is occupied at a particular energy in the microcanonical ensemble, using

$$p_i(E)=\frac{\Omega_i}{\Omega}=\sum_{s\in i,E_s^0<E}\gamma(E')_s\frac{n_s^*(E-E_s^0)^{\kappa-1}}{\Pi_{j=1}^{\kappa}h\nu_j^s}\Bigg/\sum_{E_s^0<E}\frac{n_s^*(E-E_s^0)^{\kappa-1}}{\Pi_{j=1}^{\kappa}h\nu_j^s}.$$

We calculated p_i for the sets of icosahedral and decahedral minima found for M_{75} at $\rho_0=6$. The results are given in Fig. 17. From this it can be seen that the equilibrium structure changes from decahedral to icosahedral when the total energy is only 4ϵ above the bottom of the lowest well, which corresponds to a reduced temperature of $0.018\epsilon k^{-1}$. It is likely that such a transition would not be observed until higher energies because of the energy barriers involved. In fact, this transition was observed once in an MD run started from structure 75C. The run was 10^6 time steps long and at a total energy of 74ϵ above the lowest well.

This calculation also helps to explain why 38D and 75C have not been previously reported (to the best of our knowledge) as the lowest-energy structures for the much-studied LJ potential. Global optimization algorithms are often based upon tracking the free energy global minimum as the temperature is decreased. This is the principle behind the widely used simulated annealing method.[73] However, such methods will not find the global minimum if a change in the free energy global minimum occurs at a temperature where the rate of isomerization is so low that a transition to the new structure cannot occur on the time scale of the simulation.

We should not conclude from the above calculation, though, that the global minimum is not important in understanding cluster structures. This example is probably an exception rather than the rule. Such a transition is only likely to occur for values of ρ_0 near a crossover in structures, and in the above example the cause is clearly the differences in the energy spectrum of minima for the two morphologies. In general, then, the global minimum provides a reasonable guide to the structural properties of a cluster, which can be usefully supplemented by a knowledge of other low-energy minima on the PES.

If there is a unique low-energy global minimum separated by a large-energy gap from higher-energy structures, it is appropriate to associate the solid-like structure of the cluster with this single minimum. This would be the case, for example, for the 55-atom icosahedron, 55B, at intermediate ranges of the potential (Table IV). For the LJ potential, microcanonical simulations have shown that the 55-atom cluster resides only in the icosahedral potential, well up to an energy of 40ϵ (measured with respect to the bottom of the icosahedral well), above which the formation of surface defects is observed, and then complete melting.[66,74–76] However, when there is a set of low-energy minima with very similar energies, at all but very low temperatures an equilibrium ensemble of clusters will contain a mixture of these isomers. It is therefore more appropriate to associate the ''structure'' with this set of minima, rather than the global minimum alone. For example, this would be the case for 55C, which has four low-energy isomers with the same n_{nn} (Table V).

In the above discussion we have been considering the equilibrium structural properties. However, we also need to consider the question of kinetic versus thermodynamic products. How important are the low potential energy structures in practice? When will they actually be found in an experiment? Van de Waal has suggested that kinetic factors could be essential in the growth of fcc rare-gas clusters and the nucleation of fcc solid from the LJ liquid.[68,77] As we noted earlier, the effect of increasing the size and decreasing the range of the potential is to increase the complexity of the PES. In particular, shortening the range of the potential increases the barrier heights for rearrangements and decreases their cooperativity.[27] This is because for a short-ranged potential the energy of an atom only depends on its local environment. The motion of an atom is likely to affect only the closest atoms. Therefore, as the range of the potential decreases the formation of glassy or amorphous clusters, rather than the lowest-energy structure, becomes more likely. Whether this is the case for the larger clusters we have studied when the potential is short ranged would require further investigation. The results for bulk C_{60} may also provide some insight into this question. When formed by vapor phase deposition, C_{60} gives an amorphous soot[78] and only forms the crystalline phase on recrystallization from benzene.

In this paper we have been considering the effect of the range of attraction of pair interactions on cluster structure. As rare gas clusters and clusters of C_{60} molecules can be reasonably modeled by pair potentials, we would expect the structures we have found at the appropriate ρ_0 to be very similar to the actual structures of these clusters. However, for metal clusters the range of the potential is only one factor influencing structure. In particular, many-body terms may also be important.[10] These terms may affect the relative surface energies of {111} and {100} faces, and so alter the energetic competition between icosahedral, decahedral, and fcc structures.[62] For example, in a study of lead clusters, cuboctahedra are always found to be lower in energy than icosahedra because the surface energies of {111} and {100} faces are nearly equal.[64]

V. CONCLUSION

We have shown how the range of the potential determines the favored structures of atomic clusters. In particular, we have identified four principal structural regimes for Morse clusters. For a very long-ranged potential the structures are highly strained, highly coordinated, spherical, and not based on any regular packing. For large sizes these structures show little order, and have similarities to the liquid-like inherent structures found at a shorter range. At intermediate ranges of the potential, icosahedral structures are dominant. As the range of the potential decreases from short to very short, first decahedral and then fcc structures dominate. These trends have been explained by considering the strain energies and the number of nearest-neighbor contacts associated with each regime. The effect of decreasing the range of the potential is to destabilize the strained structures. Increasing the size has a similar destabilizing effect on strained structures. For example, the lowest-energy structures of LJ clusters change from icosahedral to decahedral to fcc as the size increases. It is expected that the values of N for which these crossovers occur for Morse clusters are also dependent on the range of the potential, and decrease as the range of the potential is decreased. This conclusion has been confirmed in preliminary investigations, and full results will be presented elsewhere.[70] This type of size effect is also observed in the variation of the cluster melting temperature.[79] The highly

strained liquid clusters are destabilized relative to the solid as the size increases, causing the melting temperature to increase.

Our results also allow us to comment on the Stillinger and Stillinger proposed method of hypersurface deformation.[15] We have to echo the Chang and Berry caution[80] that although increasing the range of a potential does lead to a simplification of the PES it can also cause large changes in the relative stability of different minima. The global minimum when a potential is very long ranged may be very different from the global minimum at the conditions of interest.

For mixtures of spherical colloidal particles and nonadsorbing polymer, the range of the attractive interaction between the colloidal particles can be systematically varied by changing the size of the polymer.[81] This effect has been used to study experimentally the phase diagram for such colloidal systems as a function of the range of the interaction.[82,83] We know of no physically realizable system for clusters where the range of the potential could be similarly varied to cause range-induced transitions in cluster structure. However, it remains an intriguing possibility.

ACKNOWLEDGMENTS

We are grateful to the the EPSRC (J.P.K.D.) and the Royal Society (D.J.W.) for financial support.

[1] J. D. Honeycutt and H. C. Andersen, J. Phys. Chem. **91**, 4590 (1987).
[2] B. W. van de Waal, J. Chem. Phys. **90**, 3407 (1989).
[3] J. A. Northby, J. Xie, D. L. Freeman, and J. D. Doll, Z. Phys. D **12**, 69 (1989); J. Xie, J. A. Northby, D. L. Freeman, and J. D. Doll, J. Chem. Phys. **91**, 612 (1989).
[4] B. Raoult, J. Farges, M. F. de Feraudy, and G. Torchet, Z. Phys. D **12**, 85 (1989); Philos. Mag. B **60**, 881 (1989).
[5] R. W. Hasse, Phys. Lett. A **161**, 130 (1991).
[6] J. E. Jones and A. E. Ingham, Proc. R. Soc. London Ser. A **107**, 636 (1925).
[7] P. A. Braier, R. S. Berry, and D. J. Wales, J. Chem. Phys. **93**, 8745 (1990).
[8] I. Bytheway and D. L. Kepert, J. Math. Chem. **9**, 161 (1992).
[9] R. S. Berry, J. Phys. Chem. **98**, 6910 (1994).
[10] D. J. Wales, J. Chem. Soc. Faraday Trans. **86**, 3505 (1990); J. P. K. Doye and D. J. Wales, J. Chem. Soc., Faraday Trans. **88**, 3295 (1992).
[11] P. M. Morse, Phys. Rev. **34**, 57 (1929).
[12] M. R. Hoare and J. McInnes, J. Chem. Soc., Faraday Discuss. **61**, 12 (1976).
[13] M. R. Hoare and J. McInnes, Adv. Phys. **32**, 791 (1983).
[14] J. Rose and R. S. Berry, J. Chem. Phys. **98**, 3262 (1993).
[15] F. H. Stillinger and D. K. Stillinger, J. Chem. Phys. **93**, 6106 (1990).
[16] F. H. Stillinger and T. F. Weber, J. Stat. Phys. **52**, 1429 (1988).
[17] M. S. Stave and A. E. DePristo, J. Chem. Phys. **97**, 3386 (1992).
[18] M. H. J. Hagen, E. J. Meijer, G. C. A. Mooij, D. Frenkel, and H. N. W. Lekkerkerker, Nature **365**, 425 (1993).
[19] A. Cheng, M. L. Klein, and C. Caccamo, Phys. Rev. Lett. **71**, 1200 (1993); C. Caccamo, Phys. Rev. B **51**, 3387 (1995).
[20] E. Lomba and N. G. Almarza, J. Chem. Phys. **100**, 8367 (1994).
[21] M. H. J. Hagen and D. Frenkel, J. Chem. Phys. **101**, 4093 (1994).
[22] L. Mederos and G. Navascues, J. Chem. Phys. **101**, 9841 (1994).
[23] K. Shukla and R. Rajagopalan, J. Chem. Phys. **101**, 11077 (1994).
[24] P. Bolhuis and D. Frenkel, Phys. Rev. Lett. **72**, 2211 (1994); P. Bolhuis, M. Hagen, and D. Frenkel, Phys. Rev. E **50**, 4880 (1994).
[25] C. F. Tejero, A. Danoun, H. N. W. Lekkerkerker, and M. Baus, Phys. Rev. Lett. **73**, 752 (1994); A. Danoun, C. F. Tejero, and M. Baus, Phys. Rev. E **50**, 2913 (1994); C. F. Tejero, A. Danoun, H. N. W. Lekkerkerker, and M. Baus, *ibid*. **51**, 558 (1995).
[26] D. J. Wales, J. Chem. Soc. Faraday Trans. **90**, 1061 (1994).
[27] D. J. Wales, J. Chem. Phys. **101**, 3750 (1994).
[28] C. Rey, L. J. Gallego, and J. A. Alonso, Phys. Rev. B **49**, 8491 (1994).
[29] J. A. Northby, J. Chem. Phys. **87**, 6166 (1987).
[30] In Ref. 7, using $1/\beta$ as the unit of length, the unit of time was incorrectly given as $(m/4\epsilon\beta^2)^{1/2}$. In fact, it should be $(m/\epsilon\beta^2)^{1/2}$.
[31] L. A. Girifalco, J. Phys. Chem. **96**, 858 (1992).
[32] D. J. Wales and J. Uppenbrink, Phys. Rev. B **50**, 12 342 (1994).
[33] L. A. Girifalco and V. G. Weizer, Phys. Rev. **114**, 687 (1959).
[34] T. Kihara and S. Koba, J. Phys. Soc. Jpn. **7**, 348 (1952).
[35] M. R. Hoare and P. Pal, Nature Phys. Sci. **236**, 35 (1972).
[36] B. M. Smirnov, Chem. Phys. Lett. **232**, 395 (1995).
[37] I. A. Harris, R. S. Kidwell, and J. A. Northby, Phys. Rev. Lett. **53**, 2390 (1984); I. A. Harris, K. A. Norman, R. V. Mulkern, and J. A. Northby, Chem. Phys. Lett. **130**, 316 (1986).
[38] F. H. Stillinger and T. A. Weber, Phys. Rev. A **25**, 978 (1982).
[39] L. Verlet, Phys. Rev. **159**, 98 (1967).
[40] C. J. Tsai and K. D. Jordan, J. Phys. Chem. **97**, 11 227 (1993).
[41] J. P. K. Doye and D. J. Wales, J. Chem. Phys. **102**, 9659 (1995).
[42] L. T. Wille, J. Phys. A **18**, L419 (1985).
[43] C. D. Maranas and C. A. Floudas, J. Chem. Phys. **97**, 7667 (1992); **100**, 1247 (1994).
[44] D. Cvijovic and J. Klinowski, Science **267**, 664 (1995).
[45] S. Wolfram, *Mathematica*, 2nd ed. (Addison-Wesley, Redwood City, CA, 1991).
[46] R. W. Rudolph and W. R. Pretzer, Inorg. Chem. **11**, 1974 (1972).
[47] M. R. Hoare and P. Pal, Adv. Phys. **20**, 161 (1971).
[48] M. R. Hoare, Adv. Chem. Phys. **40**, 49 (1979).
[49] A. L. Mackay, Acta Cryst. **15**, 916 (1962).
[50] J. Farges, M. F. de Feraudy, B. Raoult, and G. Torchet, J. Chem. Phys. **78**, 5067 (1983); **84**, 3491 (1986); Adv. Chem. Phys. **70**, 45 (1988).
[51] M. Sung, R. Kawai, and J. H. Weare, Phys. Rev. Lett. **73**, 3552 (1994).
[52] G. Wulff, Z. Krist. **34**, 449 (1901).
[53] C. L. Cleveland and U. Landman, J. Chem. Phys. **94**, 7376 (1991).
[54] M. Drechsler and J. F. Nicholas, J. Phys. Chem. Solids **28**, 2609 (1967).
[55] A. Pinto, A. R. Pennisi, G. Faraci, G. D'Agostino, S. Mobilo, and F. Boscherini, Phys. Rev. B **51**, 5315 (1995).
[56] O. Echt, K. Sattler, and E. Recknagel, Phys. Rev. Lett. **47**, 1121 (1981).
[57] K. E. Schriver, M. Y. Hahn, J. L. Persson, M. E. LaVila, and R. L. Whetten, J. Phys. Chem **93**, 2869 (1989).
[58] T. D. Klots, B. J. Winter, E. K. Parks, and S. J. Riley, J. Chem. Phys. **92**, 2110 (1990); **95**, 8919 (1991).
[59] M. Pellarin, B. Baguenard, J. L. Vialle, J. Lermé, M. Broyer, J. Miller, and A. Perez, Chem. Phys. Lett. **217**, 349 (1994).
[60] O. Echt, O. Kandler, T. Leisner, W. Miehle, and E. Recknagel, J. Chem. Soc. Faraday Trans. **86**, 2411 (1990).
[61] S. Ino, J. Phys. Soc. Jpn. **27**, 941 (1969).
[62] J. Uppenbrink and D. J. Wales, J. Chem. Phys. **96**, 8520 (1992).
[63] Q. Wang, M. D. Glossman, M. P. Iniguez, and J. A. Alonso, Philos. Mag. B **69**, 1045 (1994).
[64] H. S. Lim, C. K. Ong, and F. Ercolessi, Surf. Sci. **269/270**, 1109 (1992).
[65] L. D. Marks, Philos. Mag. A **49**, 81 (1984).
[66] F. H. Stillinger and D. K. Stillinger, J. Chem. Phys. **93**, 6013 (1990).
[67] J. P. K. Doye and D. J. Wales, in preparation.
[68] B. W. van de Waal, J. Chem. Phys. **98**, 4909 (1993).
[69] T. P. Martin, U. Näher, H. Schaber, and U. Zimmerman, Phys. Rev. Lett. **70**, 3079 (1993).
[70] J. P. K. Doye and D. J. Wales (in preparation).
[71] D. J. Wales, Mol. Phys. **78**, 151 (1993).
[72] G. Franke, E. R. Hilf, and P. Borrmann, J. Chem. Phys. **98**, 3496 (1993).
[73] S. Kirkpatrick, C. D. Gelatt, and M. P. Vecchi, Science **220**, 671 (1983).
[74] H-P. Cheng and R. S. Berry, Phys. Rev. A **45**, 7969 (1992).
[75] R. Kunz and R. S. Berry, Phys. Rev. Lett. **71**, 3987 (1993); Phys. Rev. A **49**, 1895 (1994).
[76] J. P. K. Doye and D. J. Wales, J. Chem. Phys. **102**, 9673 (1995).
[77] B. W. van de Waal, Phys. Rev. Lett. **67**, 3263 (1991).
[78] W. Krätschmer, L. D. Lamb, K. Fostiropoulos, and D. R. Huffman, Nature **347**, 354 (1990).
[79] T. Ben David, Y. Lereah, G. Deutscher, R. Kofman, and P. Cheyssac, Philos. Mag. A **71**, 1135 (1995).
[80] X-Y. Chang and R. S. Berry, J. Chem. Phys. **97**, 3573 (1992).
[81] A. P. Gast, C. K. Hall, and W. B. Russel, J. Colloid. Interface Sci. **96**, 251 (1983).
[82] F. Leal Calderon, J. Bibette, and J. Biais, Europhys. Lett. **23**, 653 (1993).
[83] P. N. Pusey, W. C. K. Poon, S. M. Illett, and P. Bartlett, J. Phys. Condens. Matter A **6**, 29 (1994).